AAPS PharmSciTech, Vol. 16, No. 4, August 2015 (© 2014)
DOI: 10.1208/s12249-014-0271-z

Research Article

A Menthol-Based Solid Dispersion Technique for Enhanced Solubility and Dissolution of Sulfamethoxazole from an Oral Tablet Matrix

Bibi F. Choonara,[1] Yahya E. Choonara,[1] Pradeep Kumar,[1] Lisa C. du Toit,[1] Lomas K. Tomar,[1] Charu Tyagi,[1] and Viness Pillay[1,2]

Received 11 November 2014; accepted 10 December 2014; published online 31 December 2014

Abstract. A menthol-based solid dispersion was designed to improve the intrinsic solubility of the poorly soluble sulfamethoxazole- a class II drug molecule of Biopharmaceutics Classification System (BCS) displaying widespread antibacterial activity. Solid dispersions of menthol and sulfamethoxazole were compressed with hydroxypropyl methylcellulose (HPMC) into suitable sulfamethoxazole-loaded matrix tablets for oral drug delivery. The sulfamethoxazole-loaded solid dispersions and compressed tablets were characterized for their physicochemical and physicomechanical properties such as changes in crystallinity, melting point, molecular transitions, and textural analysis for critical analysis of their effects on the solubility and dissolution of sulfamethoxazole. The formulations were further evaluated for swelling, degradation, solubility, and *in vitro* drug release behavior. *In vitro* drug release from the sulfamethoxazole-loaded matrix tablets displayed a minimum and maximum fractional release of 0.714 and 0.970, respectively. The tablets further displayed different release rate profiles over the study periods of 12, 16, 48, and 56 h which were attributed to the varying concentrations of menthol within each formulation. Menthol was determined as a suitable hydrophilic carrier for sulfamethoxazole since it functioned as a solubilizing and release-retarding agent for improving the solubility and dissolution of sulfamethoxazole as well as controlling the rate at which it was released.

KEY WORDS: crystallinity; menthol; oral solubility and dissolution; solid dispersion; sulfamethoxazole.

INTRODUCTION

The aqueous solubility of a drug molecule is a major pharmaceutical formulation challenge as it is critical for achieving optimal oral bioavailability (1). Various approaches have been explored for improving the solubility of poorly soluble drug molecules such as sulfamethoxazole (SMX). SMX was selected for this study as it is a bacteriostatic antibiotic within the sulfonamide class of drugs with activity against a wide range of organisms including susceptible strains of *Staphylococcus aureus*, *Streptococcus*, *Haemophilus influenza*, *Escherichia coli*, and *Enterobacter* (2). SMX is commonly used in combination with trimethoprim for urinary tract infections (UTIs) (2). Due to its limited aqueous solubility (610 mg/L at 37°C), SMX is used at high doses which facilitates the development of resistance and as a result poses a significant drawback (2).

The modification of the physicochemical property of the molecule, the use of supercritical fluid processes, surfactants, solubilizers, and novel excipients are some of the approaches used to improve solubility of poorly soluble drug molecules (1,3–5). Modification of the physicochemical property of a molecule includes the reduction of the particle size to increase the surface area through micronization and nanosuspensions as well as crystal engineering to decrease the crystallinity through the formation of solid dispersions (1,6). Chemical modification of a molecule comprises techniques such as change in pH, complexation, and salt formation (1). Although the reduction in particle size is most commonly used, it often imparts an inordinate amount of physical stress on the drug molecule that results in degradation especially for thermosensitive and unstable molecules (1). Solid dispersions have been considered as one of the most promising approaches to enhance the solubility, dissolution, and subsequent oral bioavailability of poorly soluble drugs through various techniques (1,6).

Typically, solid dispersions refer to a group of solid products consisting of two different components (7,8). The two components are generally a hydrophobic drug, molecularly dispersed within a hydrophilic polymer which may be crystalline or amorphous in nature (9). Solid dispersions can be classified into five main categories, namely simple eutectic mixtures, amorphous precipitations in a crystalline matrix, solid solutions, glass suspensions, and glass solutions (7). Sekiguchi and Obi (10) first demonstrated the use of solid dispersions by creating a eutectic mixture for the delivery of the sulfonamide drug, sulfathiazole (aqueous solubility= 373 mg/L at 25°C). Subsequently, Levy (11) established a basic

[1] Wits Advanced Drug Delivery Platform Research Unit, Department of Pharmacy and Pharmacology, School of Therapeutic Sciences, Faculty of Health Sciences, University of the Witwatersrand, Johannesburg, 7 York Road, Parktown, 2193, South Africa.
[2] To whom correspondence should be addressed. (e-mail: viness.pillay@wits.ac.za)

and precise method for the preparation of solid dispersions and solid solutions. Conclusive results from both studies displayed the improvement of solubility and dissolution by the use of solid dispersions. Since its innovation in 1961, solid dispersions have become the cornerstone for improvement in the oral delivery of poorly water-soluble drugs today (12).

Solid dispersions for the improvement of poorly soluble SMX have not been investigated, and thus the aim of this study was to improve the solubility and dissolution rate of SMX through the formation of a menthol-based solid dispersion. According to the Biopharmaceutics Classification System (BCS), SMX is classified as a class II molecule with poor solubility and high permeability (13,14). SMX has limited solubility in water but is optimally soluble in alcohol, acetone, and alkali hydroxides (15). Thus, this system demonstrates the solubility improvement of SMX through the use of hydrophilic menthol. SMX-loaded matrix tablets of the solid dispersions of menthol and SMX were formulated to significantly improve the oral delivery of SMX. This system may potentially decrease the dose required to achieve a therapeutic effect and improve resistance rates. The physicochemical and physicomechanical characteristics of the system as well as the solubility and *in vitro* evaluation of the solid dispersions have been investigated and presented in this paper.

MATERIALS AND METHODS

Materials

Menthol (2-isopropyl-5-methylcyclohexanol, 99% purity, M_W=156.27 g/mol), (hydroxypropyl)methyl cellulose (Methocel, viscosity grade = 2%), sulfamethoxazole (SMX) (M_W=253.28 g/mol), and excipients such as sodium carboxymethyl cellulose (CMC) and magnesium stearate were purchased from Sigma-Aldrich Corp. (St. Louis, MO, USA). All other materials were of analytical grade and were employed as received.

Preparation of the SMX-Loaded Solid Dispersions

Solid dispersions were prepared according to a co-melt method, involving the combination of menthol and SMX by a heating and mixing process as proposed by Arnikar *et al.* (47). The upper (10 g) and lower (1 g) limits of menthol for achievement of a solid dispersion were determined based on preformulation studies. Various concentrations were selected within these limits as shown in Table I. In addition, since SMX had an experimental aqueous solubility of 610 mg/L at 37°C, an excess of ±10 mg/mL was utilized to determine the improvement in solubility of SMX when formulated as a solid dispersion. Based on the upper and lower limits determined from preformulation studies, various concentrations of menthol were heated using a heated magnetic stirrer to a temperature of 37±0.5°C until a liquid melt was obtained. SMX (50 mg) was subsequently added to the liquid melt (±5 mL) and heated to a temperature of 160± 0.5°C to enable the melting of SMX. The physical mixtures underwent constant magnetic stirring at a speed of 300 rpm for ±30 min (maintained at a temperature of 160±0.5°C) until homogenous solid dispersions were formed. Thereafter, a 5% (*w*/*w*) concentration of a cryoprotectant (sucrose) was added in equal volume to the solid dispersion. The resultant solid dispersions were placed in a freezer at −80°C for 24 h. Thereafter, the frozen SMX-loaded solid dispersions were lyophilized (Labconco Freeze-Dry Systems, Labconco Corp., Kansas City, MO, USA) for 48 h to form freeze-dried SMX-loaded solid dispersion powders for physicochemical and physicomechanical characterization. Typically, lyophilization is used as a method for the sublimation of menthol from a formulation; however, the high percentage of cryoprotectant that was added to the solid dispersion was used to protect the menthol from freezing and desiccation stresses during the lyophilization process (16–18). As a result, excess menthol was absorbed onto the cryoprotectant thereby minimizing processing losses. The lyophilized solid dispersions were then combined with 100 mg of hydroxypropyl methylcellulose (HPMC), 12 mg of CMC, and 1 mg of magnesium stearate before compression at 5 t to form SMX-loaded matrix tablets with dimensions of ~10 mm×4.5 mm (diameter × thickness) using a Carver Tableting Press (Wabash, Indiana, USA).

Table I. Solid Dispersions Synthesized Using the Co-Melt Method

Formulation no.	Menthol (g)	Sulfamethoxazole (mg)
1	1	50
2	4	50
3	4.5	50
4	5	50
5	5.5	50
6	6	50
7	10	50

In-Process Validation of the SMX-Loaded Solid Dispersions and the SMX-Loaded Matrix Tablets

The solid dispersions were analyzed with respect to their physical appearance, particle size, and powder flow properties while the matrix tablets were evaluated for their uniformity in mass, thickness, and friability. The physical appearance was assessed based on color and texture, and the average particle size was determined by Zetasizer Nano ZS (Malvern Instruments Ltd., UK). The samples were thoroughly dispersed in 10 mL of distilled water prior to filtering 2 mL of the sample through a 0.22 μm pore filter into a cuvette for analysis by Zetasizer. Measurement of the angle of repose and Carr's compressibility index was used to classify the flow properties of the lyophilized SMX-loaded solid dispersions. The weight of each matrix tablet was determined using an analytical digital balance (Mettler, Model AE 240, Griefensee, Switzerland), while the thickness of the matrix tablets were determined using a digital caliper (25×0.01 mm capacity) (Taizhou Hangyu Tools Gauge And Blades Co., Ltd., Wenqiao, Zhejiang, China). The friability was determined on a Friabilator (Erweka D-63150, Heusenstamm, Germany) at 25 rpm for 4 min with 1% set as the upper limit of acceptability.

Thermal Analysis of the SMX-Loaded Solid Dispersions

Thermal analysis was performed on each of the SMX-loaded solid dispersions using temperature-modulated differential scanning calorimetry (TMDSC) (Mettler Toledo, DSC1, STARe System, Schwerzenback, Switzerland) to determine a change in the melting point of SMX when formulated as a solid dispersion. Accurately weighed samples (10±0.25 mg) were placed in perforated 40 μL aluminum crucibles which

were hermetically sealed and ramped between a temperature range of 25–240°C at a constant rate of 10°C/min with a constant purge of N_2 atmosphere. The glass transition temperature (T_g), onset of melting (T_o), melting peak temperature (T_p), heat of fusion (ΔH_m), and temperature of crystallization (T_c) were determined for each of the native molecules and the SMX-loaded solid dispersions. Thermogravimetric analysis (TGA) was used to determine the thermal degradation of the SMX-loaded solid dispersions upon heating. A thermogravimetric analyzer (TGA) (PerkinElmer TGA 4000, Llantrisant, Wales, UK) was used, and samples were prepared by weighing 5 mg of lyophilized powders within ceramic crucibles. The weights were tarred prior to running the samples and were heated from 25 to 900°C at a rate of 10°C/min with a constant purge of N_2 atmosphere.

Determination of Molecular and Vibrational Transitions of the SMX-Loaded Solid Dispersions

ATR-FTIR spectra were obtained for the native molecules, menthol and SMX, as well as the different concentrations of SMX-loaded solid dispersions to determine the presence of menthol and SMX within the solid dispersion. PerkinElmer Spectrum 2000 FTIR spectrophotometer with a single-reflection diamond MIRTGS detector (PerkinElmer Spectrum 100, Llantrisant, Wales, UK) was used. Samples were prepared and placed on the diamond crystal and processed by universal ATR polarization accessory for the FTIR spectrum series at a resolution of 4 cm^{-1}. Samples were analyzed between a scanning range of 4000 and 650 cm^{-1} at a constant pressure of 120 psi with 32 accumulations.

Determination of Matrix Hardness, Matrix Resilience, and Deformation Energy of the SMX-Loaded Matrix Tablets

The SMX-loaded matrix tablets were analyzed with respect to matrix resilience (MR), matrix hardness (MH), and deformation energy (DE) to determine their structural integrity. A calibrated texture analyzer (TA.XTplus, Stable Microsystems, Surrey, UK) fitted with a flat-tipped steel probe (2-mm diameter) was used for the determination of MR, MH, and DE values. Data was captured at a rate of 200 points per second using Texture Exponent Software (V3.2). MR was computed as a percentage of the ratio between the area under the curve (AUC) of the peak to baseline (AUC_{2-3}) and the baseline to peak (AUC_{1-2}) from a force-time profile as displayed in Fig. 1. The MH and DE values were both obtained from the gradient and AUC of the force-distance profiles, respectively.

The MH was calculated using the Brinell hardness number (BHN) (Eq. 1). Textural analysis on all the SMX-loaded matrix tablets was performed in triplicate. The parameters employed for the analysis are listed in Table II.

$$\mathrm{BHN} = \frac{2F}{\pi D\left(D - \sqrt{D^2 - d^2}\right)} \tag{1}$$

Where BHN is Brinell hardness number, D is diameter of indenter (mm), F is elucidated from the gradient of the initial force and the final force obtained, and d is diameter of indentation (mm).

Qualitative and Quantitative Analysis of the Crystallinity of the SMX-Loaded Solid Dispersions

The change in the percentage crystallinity of the SMX-loaded solid dispersions compared to the native molecules, menthol and SMX, were determined using an X-ray diffractometer (XRD) fitted with a high-speed silicon strip detector and operating at 600 W X-ray source for high-resolution scanning (Rigaku Miniflex Guidance 600 W, Tokyo, Japan). This characterization test was used to determine the change in crystallinity of the native molecules as compared to the SMX-loaded solid dispersions. Samples were prepared by weighing ±10 mg of lyophilized powders and placing them in aluminum sample holders. Each sample ran between an operating range of 0 and 80° 2-theta. Data was captured and analyzed using the Rigaku Powder Diffraction Analysis Software (PDXL2). Similarity of diffraction patterns, peak positions, and percentage crystallinity were determined from the various profiles obtained.

Morphological Characterization of the SMX-Loaded Solid Dispersions

The surface morphology of the SMX-loaded solid dispersions were observed using a scanning electron microscope (SEM) (FEI Company, Hillsboro, Oregon, USA) to determine characteristic changes in their crystalline and amorphous structures. Samples were fixated on aluminum stubs and sputter coated with gold for 60 s using a SPI-Module™ Sputter Coater (SPI Supplies, Structure Probe, West Chester, PA). Samples were then placed in the FEI Phenom™ scanning electron microscope operated at 10 kV in the electron imaging mode and observed at varying degrees of magnification.

Degree of Swelling and Erosion of the SMX-Loaded Matrix Tablets

The degree of swelling of the SMX-loaded matrix tablets was determined using the weight gain method (19). Tablets were weighed initially and placed in 50 mL of buffer at pH 6.8 over a period of 24 h. At predetermined time intervals (0, 1, 2, 3, 6, 8, 12, 16, 24 h), the samples were removed and reweighed to determine changes in swelling. The degree of swelling at each time interval was determined using Eq. 2. Erosion studies were conducted on the same samples after 24 h by drying to a constant weight. The percentage erosion was calculated using Eq. 3.

$$\%\ \Delta\,\mathrm{Swelling} = \frac{W_f - W_i}{W_i} \times 100 \tag{2}$$

Where W_f is the weight of the swollen tablet at time t and W_i is the initial weight of the tablet (N=3).

$$\%\ \mathrm{Erosion} = \frac{W_i - W_f}{W_i} \times 100 \tag{3}$$

Where W_i is the initial weight of the tablet and W_f is the final dried weight of the tablets after 24 h (N=3).

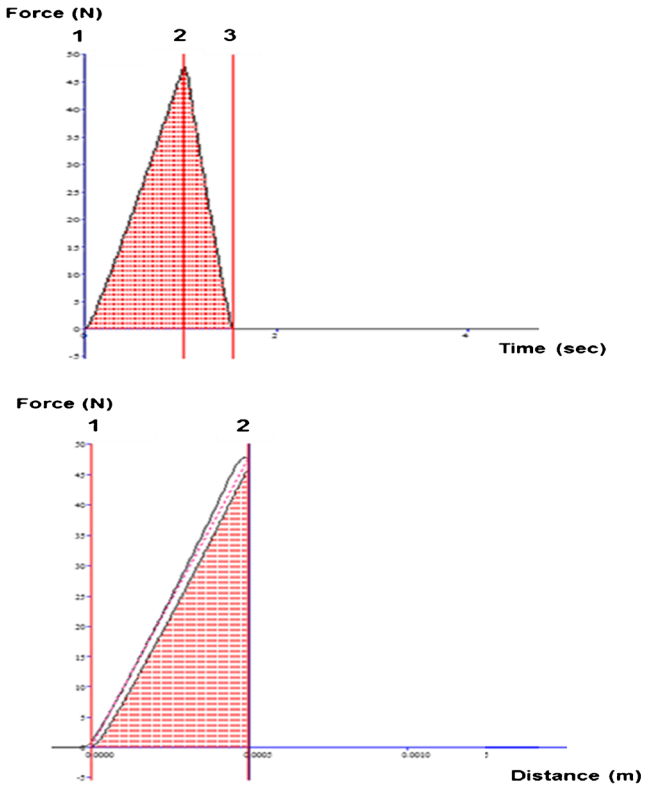

Fig. 1. Typical force-time and force-distance profiles for determination of MR (force-time profile; AUC_{2-3}/AUC_{1-2}), MH (gradient of a force-distance profile), and DE (AUC of a force-distance profile)

Determination of the Comparative Solubility of SMX and SMX-Loaded Solid Dispersions

The solubility of SMX was determined by separately dissolving 50 mg of SMX in 20 mL of menthol and simulated human intestinal fluid (SHIF) at pH 6.8 maintained at 37± 0.5°C with constant magnetic stirring (300 rpm) for 48 h. SMX-loaded solid dispersions as listed in Table I were similarly dissolved in SHIF (pH 6.8) to determine the change in solubility of the solid dispersions as compared to the pure SMX dissolved in simulated intestinal medium. Sampling of 3 mL was undertaken after 48 h, and the SMX content was determined using a UV spectrophotometer, at a wavelength of 271 nm (Implen Nanophotometer™, Implen GmbH, München, Germany). All samples were filtered using a 0.45 μm membrane filter prior to UV analysis.

Table II. Textural Profiling Parameters Used for Determining the Matrix Hardness, Matrix Resilience, and Deformation Energy of the SMX-Loaded Matrix Tablets

Parameters	Matrix hardness	Matrix resilience	Deformation energy
Pre-test speed	1 mm/s	1 mm/s	1 mm/s
Test speed	0.5 mm/s	0.5 mm/s	0.5 mm/s
Post-test speed	1 mm/s	10 mm/s	10 mm/s
Trigger type	Auto	Auto	Auto
Trigger force	0.05 N	0.05 N	0.05 N
Compression strain	N/A	40%	N/A

N/A Not available

In Vitro Drug Release from SMX-Loaded Matrix Tablets

In vitro drug release studies were performed using a USP35 dissolution apparatus II (Caleva, Model 7ST, UK). The SMX-loaded matrix tablets were placed in 900 mL SHIF at pH 6.8. Each tablet was placed beneath a ring mesh assembly within the dissolution vessel to prevent floatation. Dissolution was performed at a speed of 50 rpm (37±0.5°C). Sampling of 3 mL was undertaken at predetermined time intervals (0, 1, 2, 3, 6, 8, 10, 12, 16, 24, 48, 56 h) and replaced with an equal quantity (3 mL) of drug-free dissolution medium to maintain sink conditions. The quantity of SMX released was determined using a UV spectrophotometer at a wavelength of 271 nm (Implen Nanophotometer™, Implen GmbH, München, Germany). All samples removed were filtered using a 0.45 μm membrane filter prior to UV analysis. Drug release was calculated as a mean of three determinations as all studies were conducted in triplicate. In addition, the mean dissolution time (MDT) (Eq. 4) was calculated from dissolution data to determine the drug release rate (20).

$$\mathrm{MDT} = \frac{\sum_{i=1}^{i=n} t_{\mathrm{mid}} \times \Delta \mathrm{M}}{\sum_{i=1}^{i=n} \Delta \mathrm{M}} \tag{4}$$

Where MDT is mean dissolution time, i is the dissolution sample number, n is the number of dissolution sample time, t_{mid} is time at mid-point between i and i=1, and ΔM is the additional amount of drug dissolved between i and i=1.

In addition, the drug release data was fitted into various mathematical modeling equations in order to elucidate the mechanism of drug release.

RESULTS AND DISCUSSION

In-Process Validation Analysis of the SMX-Loaded Solid Dispersions and Matrix Tablets

SMX-loaded solid dispersions were prepared in accordance with the varying concentrations listed in Table I. The lyophilized SMX-loaded solid dispersions were successfully formulated and produced white crystalline powders with an average particle size of 110 nm with a minimum and maximum particle size of 90 and 200 nm, respectively. The powder flow properties of the SMX-loaded solid dispersions were determined using the angle of repose and Carr's compressibility index. The average Carr's compressibility index and angle of repose of the SMX-loaded solid dispersions were 9.17% and 19.29°, respectively. The minimum and maximum values of the solid dispersions for Carr's compressibility index were 8.93 and 9.21%, whereas the angle of repose was 18.99 and 19.54°. According to McGlinchey (21), the values obtained indicated excellent powder flow properties as they fall within the range of 5–15% for Carr's compressibility index and <20° for angle of repose. The SMX-loaded matrix tablets were evaluated for uniformity of mass, thickness, and friability. All the SMX-loaded matrix tablets were uniform in mass, each having an average weight of 550±0.5 mg. The

thickness ranged from 4.5±0.05 to 5.1±0.03 mm while the friability was at an average of 0.7% (*i.e.* within the set limit 1%), demonstrating desirable compressibility and resistance to chipping.

Thermal Analysis of the SMX-Loaded Solid Dispersions

SMX and menthol are pure, low molecular weight molecules (<500 g/mol), and thus the onset of melting (T_o) was considered as the melting temperature (T_m) (22). In addition, between the T_o and T_p (melting peak), the sample continues to melt (22). The TMDSC thermograms of SMX and menthol are depicted in Fig. 2a. SMX displayed a single, narrow, defined peak with an onset of melting (T_o) at 169.02°C which corresponded to the melting temperature (T_m). The quantity of heat per unit mass that was required to change the SMX from a solid to liquid at its melting point was 120.92 J g^{-1}. In contrast, menthol displayed a heat of fusion (ΔH_m) of

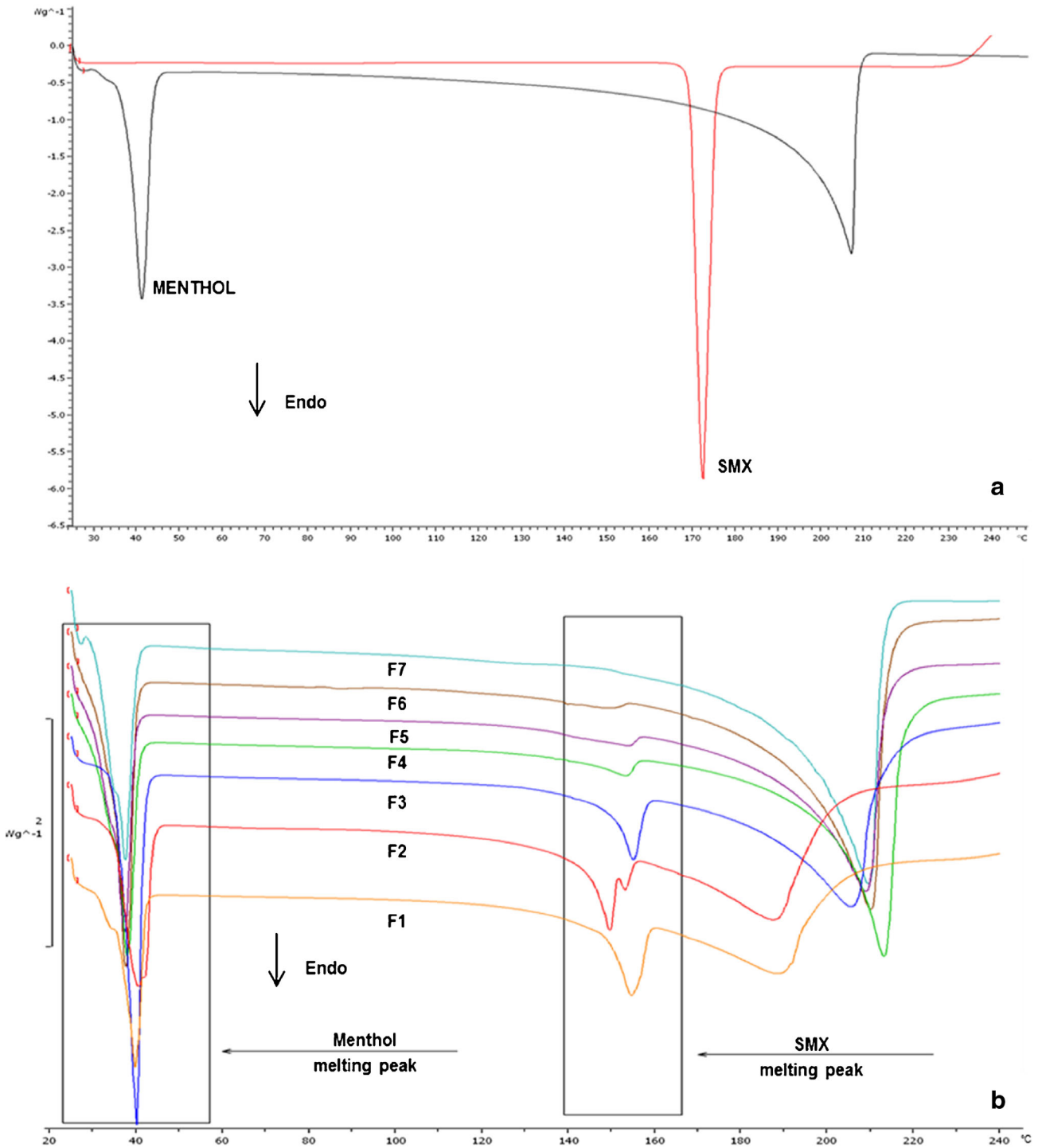

Fig. 2. TMDSC thermal profiles for **a** native SMX and menthol and **b** SMX-loaded solid dispersions F1–7

79.62 J g^{-1} with a melting onset at 37.19°C and a T_p at 40.44°C. The first endothermic shift that was noticed for menthol was indicative of the glass transition temperature (T_g) at approximately 28.36°C and corresponded to the softening of the menthol (23). In addition, another endothermic event was observed in the TMDSC thermogram for menthol at a temperature of 205.97°C confirming a phase change (sublimation) since menthol has a boiling point of 212°C (24).

On comparison of the TMDSC thermograms of the individual molecules with the SMX-loaded solid dispersions, a predictable melting peak was noticeable between 37 and 40°C for all formulations. The first endothermic events for F1–7 (Fig. 2b) were identical to the peak observed for the individual menthol, thus indicating the melting of menthol within these formulations. Consequently, the endothermic event between 195.89 and 216.77°C in F1–7 was characteristic of the sublimation of menthol. The reduction in intensity and the shifting of the sharp melting peak of SMX in the solid dispersions were noticeable for F1–7. F1–3 (Fig. 2b) displayed melting endotherms similar to the endothermic peak of SMX with a melting temperature of 149.24, 145.32, and 150.48°C, respectively. Analysis of the SMX melting peak in F1–7 showed the successive decrease in intensity. This corresponded to the decreased ΔH_m observed for each of the formulations with F1 showing the highest value (22.68 J g^{-1}), F6 displaying the lowest value (1.12 J g^{-1}), and F7 showing a complete absence of the drug peak. It was speculated that the decrease in intensity of the SMX peak is attributed to the dissolving of SMX within the melted menthol during DSC measurements and as a result, distinct endothermic peaks corresponding to the melting of menthol was observed (25–27). In addition, the results may indicate that the degree of crystallinity was substantially reduced and the SMX was present in an amorphous form within the solid dispersion, thus accounting for the reduced intensity and shifting peaks (25,26).

The results obtained for DSC were analogous to existing data that depicted the absence of drug peaks in the thermograms of solid dispersions of the poorly water-soluble drugs, tacrolimus and piroxicam (25,28). This was attributed to its dissolution within the melted carrier during DSC measurements and only displayed the appearance of an endothermic peak corresponding to the melting of the carrier (25,28).

The TGA profiles of SMX and menthol displayed the change in mass of the native molecules as a function of temperature (Fig. 3a). Upon heating the samples, SMX displayed a stepped decrease in percentage weight with an initial loss of 21.827% at a temperature of 301.92°C. Subsequently, as the temperature increased to 400°C, a 50% decrease in sample weight was noticed, and at the end of the temperature range (894.87°C), only 27% of the sample had remained. In contrast, menthol displayed a complete decrease in mass of 99.092% at 194.27°C which was attributed to the vaporization of the menthol (29). The TGA profiles of the native molecules were compared to the SMX-loaded solid dispersions, and the differences were noted (Fig. 3b). F1 depicted a similar stepped, but significantly larger decrease (97.869%) in the mass as compared to SMX. All the other curves were representative of F2–7 (Fig. 3b). The curves displayed were characteristically similar to menthol, displaying a significant mass loss (±90%) within the temperature range of 188.30–203.85°C. These results corresponded to the decreased intensity of the SMX peaks and the prominent menthol peaks observed in the TMDSC thermograms. In summary, the concentration of menthol contained within each formulation directed the thermal degradation and melting behavior of F1–7. TMDSC and TGA data confirmed the formation of a solid dispersion.

Analysis of the ATR-FTIR Spectra of the SMX-Loaded Solid Dispersions

Complete ATR-FTIR split transmittance spectra of menthol and SMX as well as the varying concentrations of SMX-loaded solid dispersions listed in Table I are shown in Fig. 4 with characteristic peaks identified. Sucrose was used as the background spectrum for FTIR measurements and was subtracted from the sample spectrum so as to gain information about the solid dispersion only. Since menthol is a terpene alcohol, it displayed a strong, broad peak at 3270 cm^{-1} which was indicative of –O-H stretching (30,31). In addition, absorption due to carbon-hydrogen stretching was observed between 2800 and 2900 cm^{-1}. At lower frequencies (1375 cm^{-1} to 1470 cm^{-1}), menthol displayed carbon-hydrogen bending typical of methyl groups present within menthol. The defining peaks of SMX were observed between a wavelength of 3000 to 3500 and 1200 to 1500 cm^{-1} which corresponded to –N-H and SO_2 stretching vibrations, respectively (30).

The distinct bands spanning from 3000 to 3500 cm^{-1} in solid dispersions F1–3 were characteristic of –N-H stretching, identical to those found in SMX. The bands were narrower and less intense than –O-H bands of alcohols and phenols and thus diagnostic of primary amide groups present (30). A decrease in peak intensity within the wavelength range of 3100 to 3200 cm^{-1} was noticeable as the concentration of menthol increased from F1 to 3, with F3 showing the largest decrease in intensity as evidenced by the increased transmittance shown in Fig. 4a. Smaller and more variable peaks appearing within the regions of 2800 to 2960 cm^{-1} in the split spectra of F1–3 indicated absorption due to –C-H stretching which occurred at the high-frequency end of the spectrum, typically indicating hybridization of the carbon (30). The bands were similar to those observed for the native molecule menthol, showing absorption peaks at 2918, 2951, 2867, and 2845 cm^{-1}. Strong absorption peaks at 1090 and 1032 cm^{-1} on the F1 spectrum, 1092 and 1030 cm^{-1} on the F2 spectrum, and 1091 and 1025 cm^{-1} on the F3 spectrum were characteristic of an overlap of primary alcohol –C-O stretching vibrations and primary amine –C-N stretching vibrations (30). Both the absorption bands were characteristically observed in the spectra for menthol and SMX, indicating the presence of both molecules within the solid dispersion.

A pair of split absorption bands centered around 1500 and 1600 cm^{-1} were present in all three spectra (F1–3) and corresponded to –C=C aromatic ring stretching vibrations, indicative of the presence of an aromatic ring which is a defining feature of SMX. The distinctive band observed at a wavelength of 1594 cm^{-1} for all three spectra F1–3 indicated δ–N-H (amide II band) stretching vibrations (30). Hetero-oxy stretching frequencies were observed within the main fingerprint spectral region of 1200–1470 cm^{-1} in spectra F1–3 with peaks observed between the ranges of 1200–1250 and 1350–1470 cm^{-1} indicating symmetrical and asymmetrical SO_2 stretching vibrations (30). This confirmed the presence of a sulphur group within the three formulations which is a determining feature of SMX.

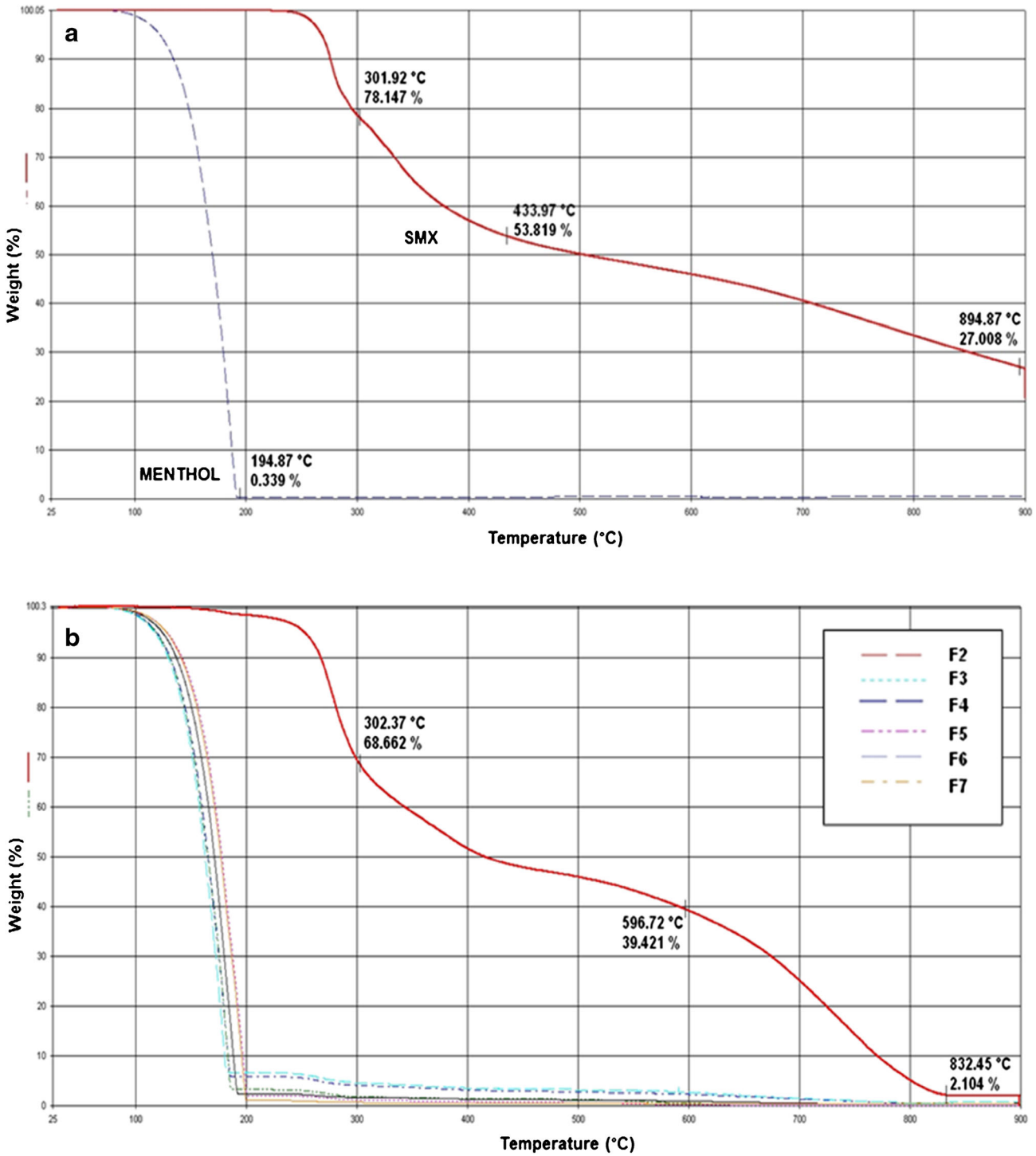

Fig. 3. TGA profiles of **a** native SMX and menthol and **b** SMX-loaded solid dispersions F1–7

FTIR absorption spectra of F4–7 had characteristic absorption bands identified which included a broad band spanning from 3200 to 3600 cm^{-1} which was as a result of the decrease in intensity and subsequent disappearance of the –N-H stretching vibrations (characteristic of the primary amide of SMX) corresponding to the increased concentrations of menthol from F4 to 7. Consequently, the appearance of the broad band indicated a hydrogen-bonded –O-H stretching vibration comparable to that of menthol. In addition, the absorption peaks that were smaller and more variable within the region 2800 to 2960 cm^{-1} for F1–3 appeared as strong distinct peaks in the split spectra for F4–7 indicating definite –C-H stretching vibrations (30).

The appearance of a new peak, uncharacteristic from either menthol or SMX, at 1735 cm^{-1} on the F4 spectrum, 1745 cm^{-1} on the F5 spectrum, 1745 cm^{-1} on the F6 spectrum,

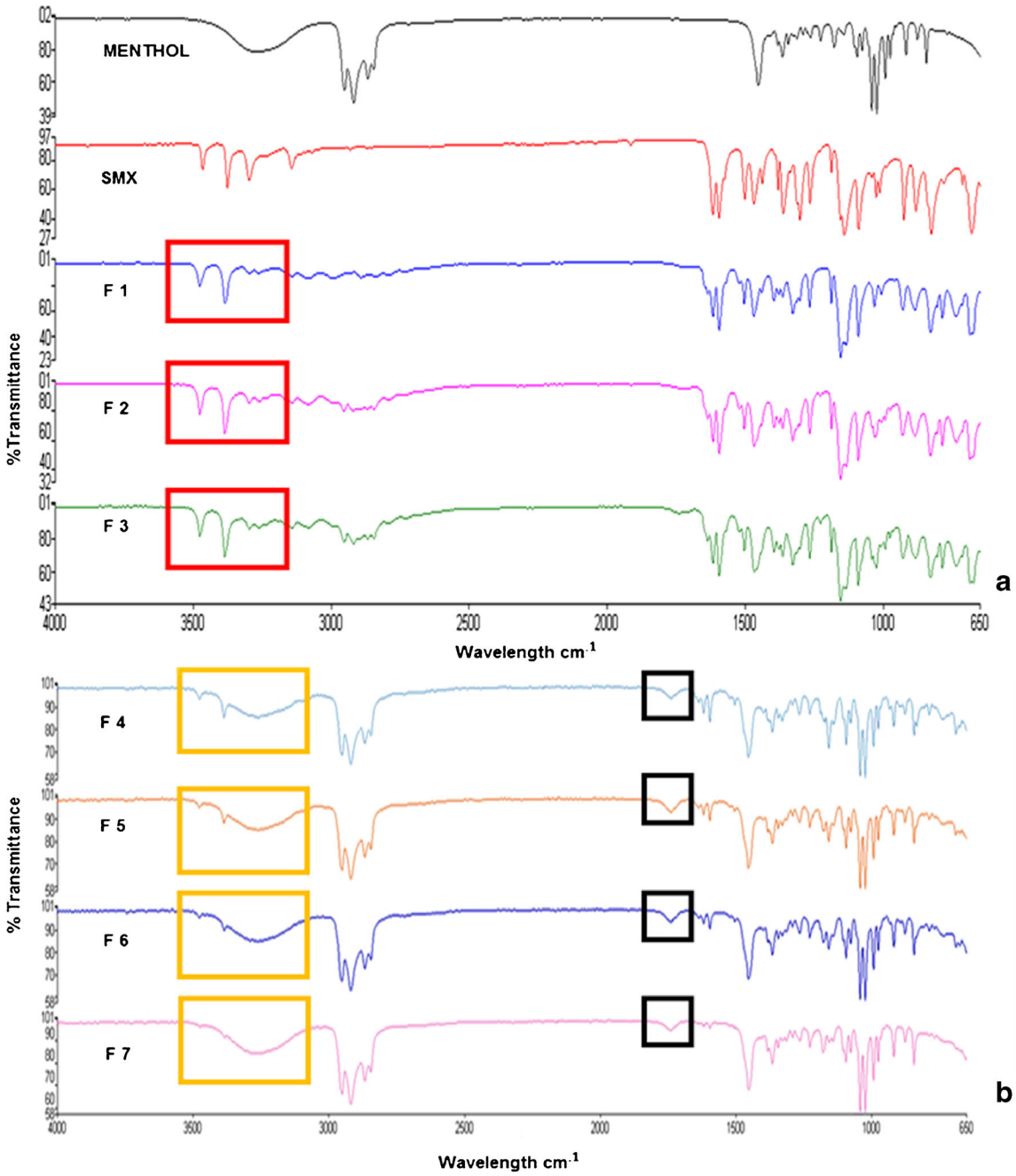

Fig. 4. ATR-FTIR transmittance spectra: **a** split spectra of menthol, SMX, and SMX-loaded solid dispersions F1–3 and **b** split spectra of SMX-loaded solid dispersions F4–7. *Red blocks* highlight the –N-H stretching vibrations (primary amide), *orange blocks* highlight the disappearance of the primary amide bond and appearance of an –O-H stretching vibration, and *black blocks* indicate –C=O stretching and formation of a new ester bond

and 1740 cm^{-1} on the F7 spectrum indicated –C=O stretching vibrations (30). This strong band represented a carboxylic acid derivative and signified intense hydrogen-bonding between the –O-H group of menthol and –C-O group of SMX (30). Although solid dispersions F1–3 depicted a peak within this region, the peak was slight and inconspicuous and thus its effect was considered unremarkable. Aromatic –C=C ring stretching and –N-H bending vibrations in the regions of 1500–1600 and 1500–1650 cm^{-1}, respectively, were present for F4–7 showing decreasing intensities as the concentration of menthol increased. Other typical peaks occurred in the range of 1000–1090 cm^{-1} due to –C-O/-C-N overlapping stretch vibrations and medium to weak δ–N-H loop bands within the region of 630–800 cm^{-1} for F4–7 (30).

Comparison of the split transmittance spectra of F1–7 clearly depicted the altered molecular and vibrational transitions as the concentration of menthol increased in relation to the constant concentration of SMX. F1–3 depicted peaks significantly alike to that of SMX, whereas F4–7 showed absorption spectrums similar to that of menthol, confirming the

increased concentrations contained within these formulations (30). However, formation of a new band and appearance of peaks characteristic to both menthol and SMX indicated successful combination of the two components in the formation of a solid dispersion (30).

Textural Profiling of the SMX-Loaded Matrix Tablets

Textural profiling of the SMX-loaded matrix tablets was performed to determine the MH, MR, and DE using force-time and force-distance profiles. MR was calculated in order to determine the ability of the matrices to return to their original dimensions after being subjected to a compression strain by the textural probe (32). The MR decreased from F1 to F3, corresponding to the decreased hardness and increased concentrations of menthol within the SMX-loaded solid dispersions. It was determined that at a consistent strain of 40%, F1 proved to be the most resilient at 55.42%, compared to the slightly lower resilience percentages for F2 (50.04%) and F3 (44.80%) (Fig. 5a). Results indicated that with higher concentrations of menthol, the flexibility of the formulations and its ability to return to its original state decreased. Accordingly, this would warrant that F4–7 would have correspondingly lower resilience values as compared to F1–3. However, this was not the case as results proved that F4 (52.80%) and F7 (57.70%) showed higher resilience values with the latter being the most resilient. This deviation was attributed to the formation of a strong hydrogen bond in F4–7 which imparted a structural flexibility typical of esters (33).

MH is a pertinent physicomechanical property essential toward controlling drug release, swelling, erosion, and matrix stability. In this study, MH was represented as an index of the ability of the matrices to resist and overcome adhesive and cohesive forces (deformation). F1 displayed the greatest hardness with a value of 240.40 N mm^2 and correspondingly high deformation energy (0.011 J), whereas F7 showed a hardness value of 55.67 N mm^2 and a correspondingly low deformation energy (0.007 J). MH decreased accordingly from F1 to 7 with increasing concentrations of menthol, creating relatively softer matrices that were more susceptible to matrix deformation.

In addition, matrix rigidity (Fig. 5b) was elucidated from the force-distance profiles of F1–7. Analysis of results depicted a predictably high matrix rigidity for F1 (95.08 N mm^2) with F2–7 displaying lower matrix rigidities. The decrease in rigidity was attributed to the distinct formation of an ester bond (Fig. 4b) within subsequent formulations leading to a less rigid structure and lower melting point as compared to the corresponding amide band (Fig. 4a) that was characteristic of SMX. In other words, as the concentration of menthol increased from F1 to 7, it resulted in the dampening of the characteristic structural features of SMX, thereby creating softer and less rigid structural matrices.

Analysis of the Crystal Nature of the SMX-Loaded Solid Dispersions

The crystallinity of the SMX-loaded solid dispersions was assessed using XRD. All spectrums that were obtained displayed to varying degrees diffraction peaks which were sharp and narrow indicating the crystallinity of the test sample and with wider and flatter peaks indicating the amorphous component. The hydrophilic carrier menthol displayed a crystallinity percentage of 30% with seven major crystalline diffraction peaks identified (Fig. 6a). Conversely, the drug molecule SMX showed 12% crystallinity with four major crystalline diffraction peaks identified on the diffraction spectra (Fig. 6b). The SMX-loaded solid dispersions were assessed according to their percentage crystallinity in relation to the native molecules, menthol and SMX.

F1 (Fig. 6c) depicted fewer diffraction peaks than menthol and SMX, displaying a high-intensity Bragg diffraction peak at ±40° 2-theta which was uncharacteristic of either menthol or SMX. F2 and F3 (Fig. 6d, e) displayed characteristic Bragg peaks at ±20° 2-theta, similar to that of SMX, with F2 showing an additional low-intensity narrow peak at ±10° 2-theta comparable to that of menthol. Bragg diffraction peaks were discernable for F4–7 (Fig. 6f–j) at ±20° 2-theta and ±10° 2-theta which was typical of the reference powder diffraction spectrums obtained for menthol and SMX. Furthermore, it was apparent that the intensities of the diffraction peaks varied with the different concentrations of menthol within each formulation.

All the SMX-loaded solid dispersions displayed decreased percentage crystallinities within the range of 11–21%. The decrease in the crystallinity observed supports the idea that modification of the physical nature of the drug through the formation of solid dispersions decreases the crystallinity and thus results in the presence of more amorphous material which has a much higher water affinity and solubility as compared to the crystalline counterpart (1,6,34). The results obtained confirmed the analysis of the TMDSC thermograms (Fig. 2b) and was consistent with the existence of a solid dispersion system. Critical analysis of XRD data on solid dispersions of carbamazepine and felodipine provided conclusive results on the potential decrease in crystallinity and presence of the amorphous state within the solid dispersion (35,36).

In addition, multivariate experimental techniques were applied to the analysis of the data obtained from DSC and XRD in order to comprehensively link the crystallinity data for the solid dispersions. Table III summarizes the crystallinity data obtained for DSC and XRD. The melting point decreases in the menthol and SMX peak noted in the solid dispersion thermograms in Fig. 2 were represented in Table III. The decrease in the melting temperature for the characteristic menthol and SMX peak indicated the increase in the amorphous constituent within the solid dispersions as compared to the crystalline counterpart and thus resulted in the easy melting of the formulation at lower temperatures (25).

Furthermore, the comparison of the XRD diffraction peaks of the native molecules with the solid dispersions depicted a decrease in intensity at the diffraction angles characterized in Table III. These broad, low-intensity peaks observed in the XRD spectrums of the solid dispersions indicated that the formulations were in the amorphous form (35). These summarized results further highlighted the expected decrease in crystallinity that is typical of solid dispersions (38, 39). In correlating the results obtained for DSC and XRD, it was noted that the solid dispersions of SMX and menthol showed a significant decrease in the endothermic peak of SMX with a similar broadening and decreased intensity of

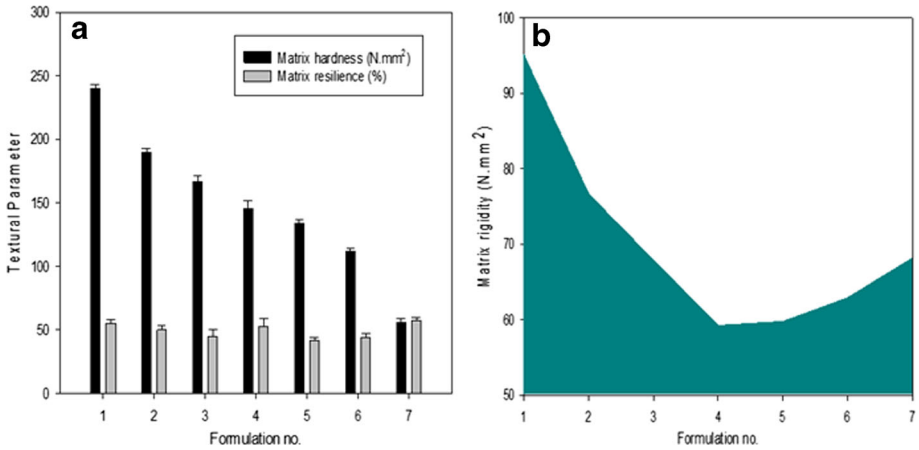

Fig. 5. Graphical representation of the **a** MH, MR, and **b** rigidity of SMX-loaded matrix tablet formulations F1–7. Significant differences noticed were F1 which achieved the highest matrix hardness (240.40 N mm^2) with the lowest concentration of menthol (1 g), and F7 achieved the lowest matrix hardness (55.67 N mm^2) with the highest concentration of menthol (10 g)

the peaks derived from SMX in the XRD data (25). This indicated the presence of the amorphous state in all the solid dispersion formulations (25).

Surface Morphological Characterization of the SMX-Loaded Solid Dispersions

The SMX-loaded solid dispersions were analyzed using SEM, and the images obtained are depicted in Fig. 7. F1 displayed largely ordered, regular, and distinct crystal forms in the SEM images (Fig. 7a, b). In contrast, F4 (Fig. 7c, d) depicted particles that were more spherical in shape with a less rugged surface structure. Furthermore, F7 (Fig. 7e, f), which contained the highest mass ratio of menthol (10 g), depicted large irregular smooth surfaces with minimal crystalline regions indicating homogeneity of the formulation. Noticeable changes were observed in the surface morphology on comparison of the various SMX-loaded solid dispersions. Most distinguishing features noted were the changes from a more rigid crystalline structure in F1 to a distinctly amorphous and smooth structure in F7. The results obtained corresponded to the decrease in crystallinity in subsequent formulations as confirmed by XRD spectra (Fig. 6). It was deduced that as the concentration of menthol increased, the surface morphology displayed characteristically amorphous regions. The appearance of amorphous regions within the SEM images confirmed the decrease in crystallinity, characteristic to solid dispersions as highlighted in the SEM micrographs obtained for the solid dispersions of carvedilol and tacrolimus (25,27).

Swelling and Erosion Studies on the SMX-Loaded Matrix Tablets

Swelling and erosion studies were performed on F1–7 of the SMX-loaded matrix tablets to obtain supplementary evidence for the observed drug release kinetics (Fig. 8). F1 swelled to ±140% of its original size in the first hour with a steady increase over the following 2 h to approximately 170% of the original mass. F2 swelled to approximately 119% of its original size in the first 3 h with both F1 and F2 showing a sharp decrease in swelling after 4 h (Fig. 8a). The swelling profile obtained for F1 and F2 accounted for the 90% erosion obtained after 24 h. F3 and F4 swelled to approximately 100 and 95% of its original size, respectively (Fig. 8a). Likewise, as for F1–2, F3–4 displayed increased erosion percentages after 24 h (Fig. 8c). The swelling profiles of F1–4 decreased steadily after approximately 4 h while F5–7 steadily increased after 4 h (Fig. 8a, b). In addition, the erosion percentage for F5–7 was <50% (Fig. 8c). All formulations displayed different swelling profiles regardless of their constant concentration of HPMC. Thus, the changes were attributed to the varying concentrations of menthol contained in each formulation.

Solubility Analysis of SMX and SMX-Loaded Solid Dispersions in SHIF

The solubility of SMX in menthol as well as SHIF at pH 6.8 was determined and compared to the solubility of each of the SMX-loaded solid dispersions in SHIF at pH 6.8. The results indicated that the solubility of SMX in menthol at 37°C was 990 μg/mL, and the solubility of SMX in SHIF at pH 6.8 (37°C) was 790 μg/mL. These results were compared to the solubility of the SMX-loaded solid dispersions (F1–7) which showed a marked increase in solubility as compared to pure SMX dissolved in SHIF at pH 6.8. Results depicted only slight differences in the solubility of pure SMX in menthol as compared to the SMX-loaded solid dispersions in SHIF at pH 6.8. F1 displayed the lowest solubility in SHIF, whereas F7 depicted the highest solubility of 998.75 and 1241.2 μg/mL, respectively (Fig. 9). F2 showed an approximate 9% increase in solubility as compared to F1. The solubility increased steadily from F3 to 6 with F7 showing a ±6% increase in solubility as compared to F6. The results displayed in Fig. 9 suggested that a proportional increase in solubility was noted with increasing concentrations of menthol. F1 and F7 depicted the lowest and highest solubility from all the formulations as they contained the lowest (1 g) and highest concentrations (10 g) of menthol, respectively. The increase in solubility of a drug molecule when formulated as a solid dispersion is highlighted extensively in literature and is a founding characteristic of solid dispersions (25–28).

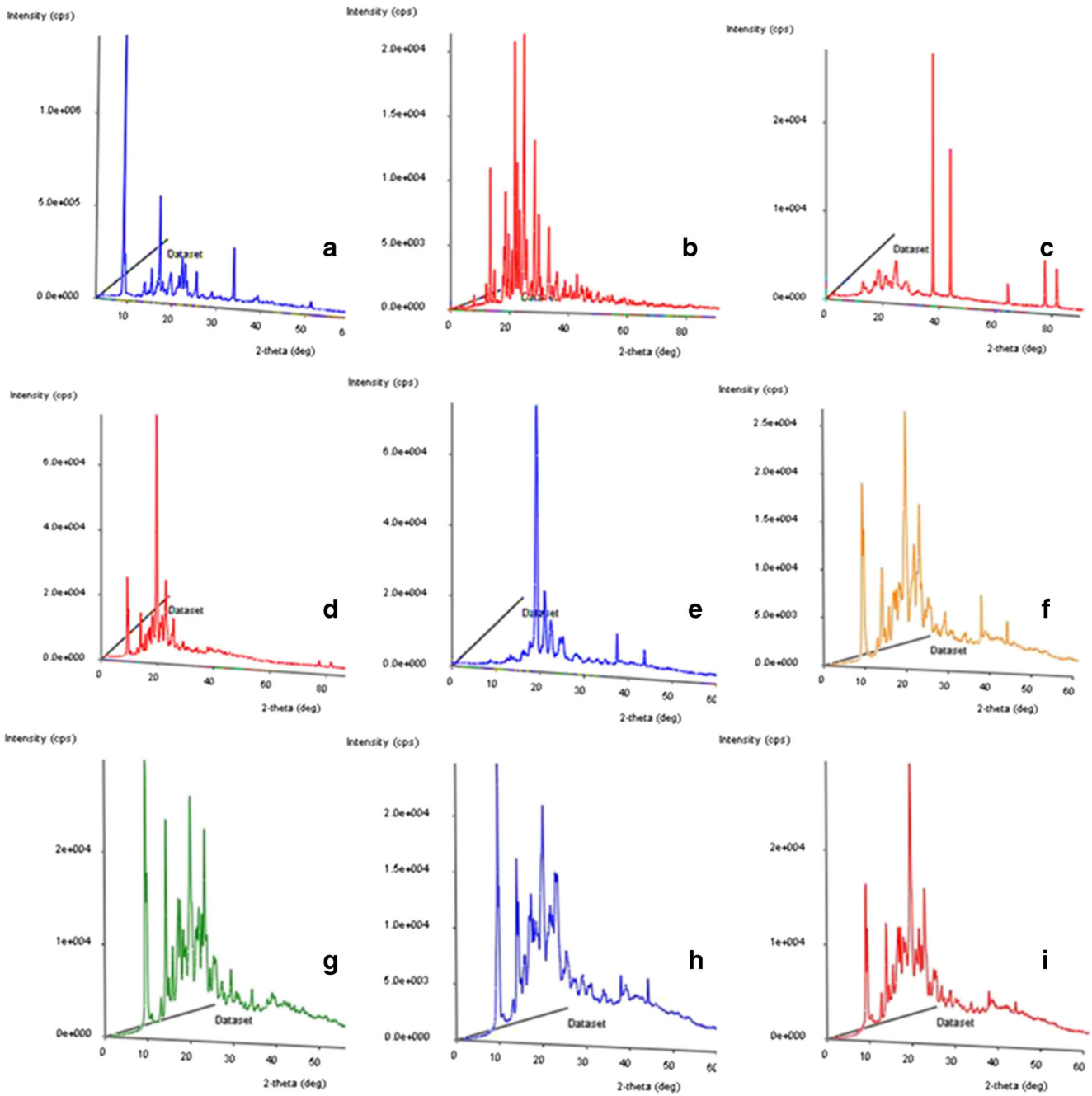

Fig. 6. XRD spectra of **a** menthol, **b** SMX, and **c–j** SMX-loaded solid dispersions F1–7. The diffraction spectrums are represented as a plot of the reflected intensities (cps) as a function of the diffraction angle 2-theta (°)

According to Vasconcelos *et al.* (9), solid dispersion directed decrease in particle size and change to an amorphous state increases the solubility of a drug molecule and thus enhances the bioavailability. The association between drug solubility, dissolution, and its subsequent increase in bioavailability is theoretically described by the Noyes-Whitney Eq. 5 (37,38):

$$\frac{dM}{dt} = \frac{DS}{h}(C_s - C) \tag{5}$$

Where M is the mass of solute dissolved in time t, $\frac{dM}{dt}$ is the mass rate of dissolution (mass/time), D is the diffusion coefficient of the solute in solution, S is the surface area of the exposed solid, h is the thickness of the diffusion layer, C_s is the solubility of the solid, and C is the concentration of solute in the bulk solution at time t.

Therefore, according to Noyes-Whitney, an increase in the solubility of a drug molecule would correspond to an increased dissolution with subsequent increase in bioavailability (38). The experimental measurements obtained showed a substantial increase in the solubility of the solid dispersions, and comparative interpretations were made in relation to the solubility of the native molecule in the same dissolution medium.

Table III. Comparative Analysis of the Crystallinity Obtained for DSC and XRD

Formulation no.	DSC melting points (°C)*	XRD diffraction peaks 2-theta (°)
F1	35.43/149.24	10–20
F2	35.82/145.32	25–40
F3	34.74/150.48	9–17
F4	33.86/145.19	23–34
F5	33.05/absent peak	30–35
F6	33.59/absent peak	20–40
F7	32.60/absent peak	23–43

*The DSC melting points are indicative of the menthol/SMX melting peak

In Vitro Drug Release Analysis

In vitro SMX release was performed in SHIF (pH 6.8), and the fractional drug release profiles of the SMX-loaded matrix tablets is presented in Fig. 10. Each formulation demonstrated diverse drug release behavior based on their varying solubility. In addition, the formulations displayed different time-release profiles. F1 and F2 released drug over a period of 12 h with the maximum release being >50% (Fig. 10a). F3 and F4 displayed prolonged release over 16 h, followed by F5 and F6 which released drug over a period of 48 h (Fig. 10b, c). F7 displayed the most prolonged drug release over a period of 56 h (Fig. 10d).

Noticeable in all the drug release profiles was the burst release which was attributed to the initial swelling within the first 3 h. Despite the decrease in swelling after 4 h for F1–4 (Fig. 8a), the drug release increased accordingly (Fig. 10a, b). This indicated that the drug release in the later phase was erosion-controlled. F5–7 (Fig. 8b) displayed a more constant swelling profile following the initial burst swelling. The swelling profile of F5–7 corresponded to the increase in drug release displayed in Fig. 10c, d. These results suggested that the release of SMX from F5–7 was swelling-controlled in contrast to F1–4. Typically, amorphous materials display increased erosion as compared to their crystalline counterparts; however, the atypical behavior observed was attributed to the distinct ester bond formation within F5–7 (Fig. 4), causing a decreased susceptibility of the solid dispersion to hydrolytic cleavage and thus slower erosion as compared to F1–4 (39).

Formulations having a higher concentration of menthol, such as F7 (10 g), depicted the highest fractional release (0.97). This paralleled the increased solubility of F7 which

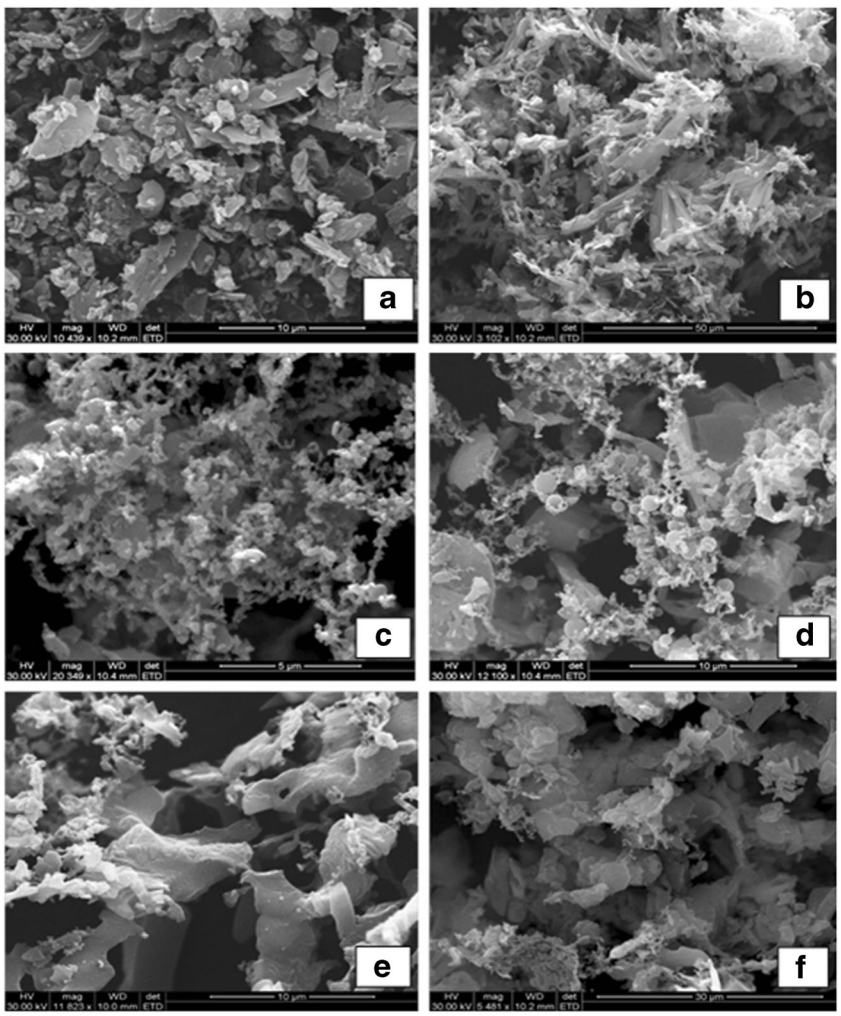

Fig. 7. SEM images at high and low magnifications for (**a**, **b**) F1, (**c**, **d**) F4, and (**e**, **f**) F7

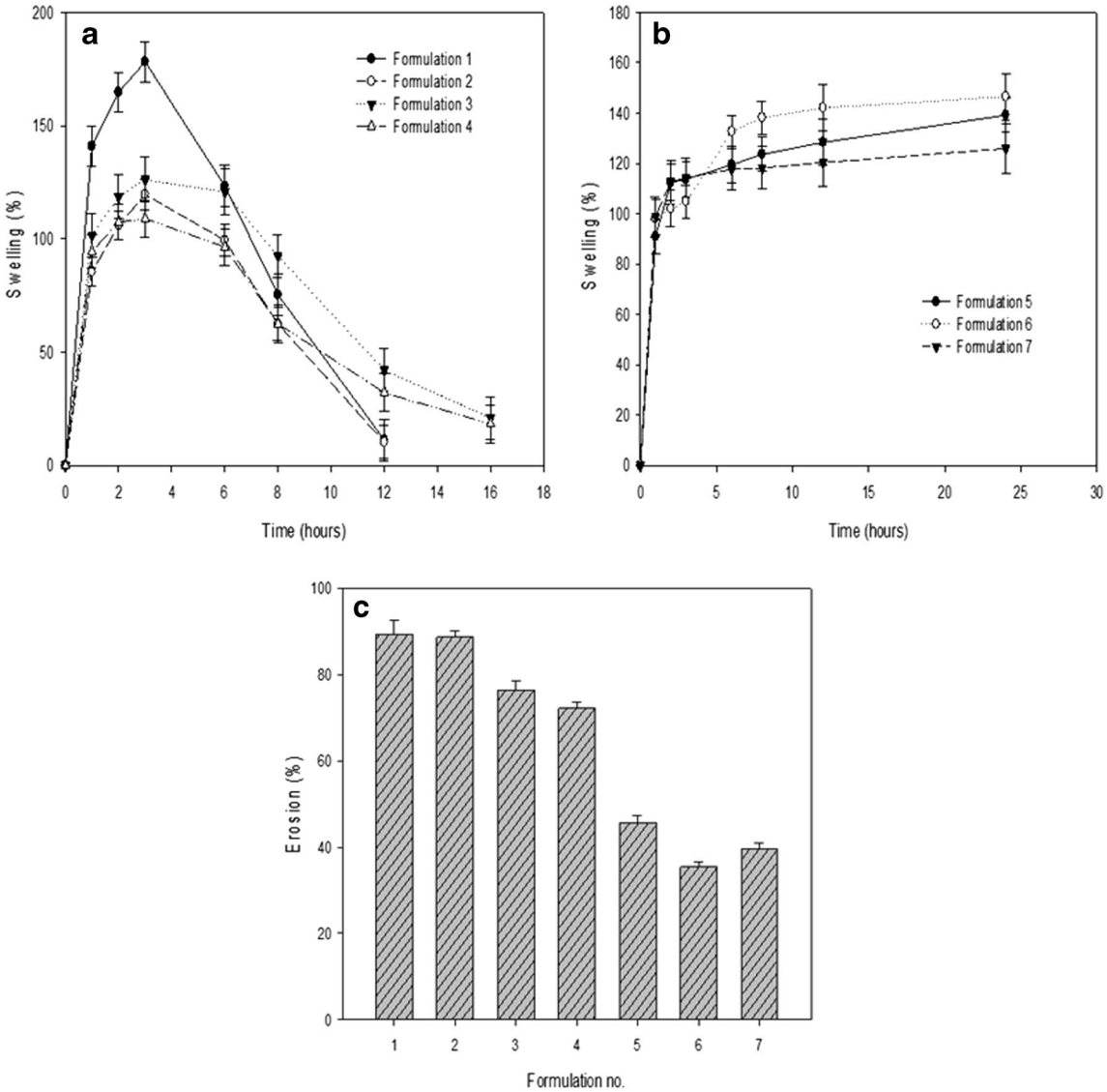

Fig. 8. Profiles depicting **a**, **b** percentage swelling over a period of 24 h for F1–7 and **c** percentage erosion for F1–F7 as a function of the dried weight of the tablets after 24 h

enabled the increased dissolution of SMX. On the other extreme, the lowest fractional release (0.71) was noticed for formulations that had lower concentrations of menthol such as F1 (1 g). Similarly, F1 had the lowest solubility in SHIF at pH 6.8 (Fig. 9). Consequently, it was concluded that the concentration of menthol used in each formulation impacted significantly on the drug release profiles obtained for the SMX-loaded solid dispersions F1–7. The solubility results (Fig. 9) correlated with the drug release profiles (Fig. 10a, d), showing that increases in solubility from F1 to 7 displayed correspondingly higher cumulative drug release percentages. The improved solubility and dissolution of the solid dispersions was attributed to the amorphization of the drug and the reduction in the particle size to the nanometer range. The particle size is inherently associated with the solubility of a drug molecule; therefore, a reduction in particle size leads to an increase in the surface area with a consequently enhanced dissolution profile (4).

Since the quantity of HPMC remained constant within each formulation, it was determined that menthol served to control the release rate of SMX from each of the SMX-loaded matrix tablets by prolonging its release as was evidenced by the mean dissolution time (MDT) obtained for F1–7. The MDT was used to depict the drug release rate from the SMX-loaded matrix tablets as well as the release-retarding ability of menthol (40,41). Overall, the MDT gave an indication of the rate of the dissolution process (20). The mean dissolution time at which 80% of drug was released (MDT_{80}) for F7 was 15.044±1.5. This was the highest MDT_{80} from all formulations, and it indicated that F7 had a higher drug release-retarding ability and thus slower release of drug as compared to other formulations. Typically, F1 and F2 had the lowest MDT_{80} of 4.592±0.5 and 5.076±0.5, respectively, and as a result the fastest release over 12 h (Fig. 10a). Thus, it was apparent that the increasing concentrations of menthol impacted on the release rate profile and served as a controlling agent that retarded drug release from the SMX-loaded matrix tablets.

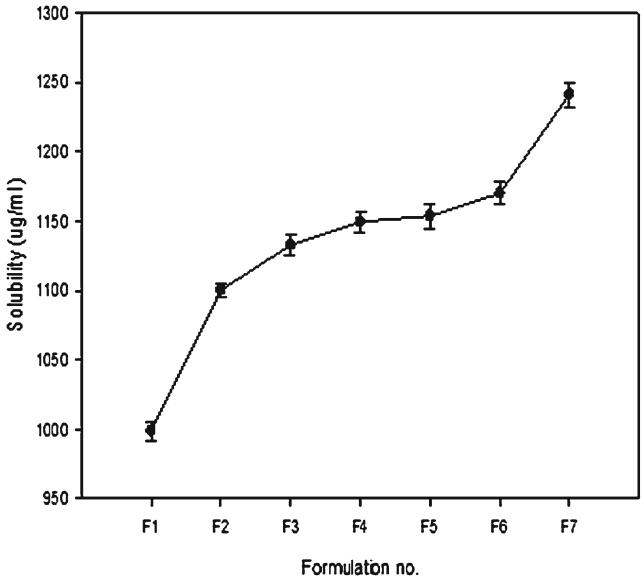

Fig. 9. Graphical representation of the solubility of SMX-loaded solid dispersions F1–7 in SHIF at pH 6.8 (37°C)

Mathematical Modeling of Drug Release Profiles

The drug release profiles of the solid dispersions F1–F7 were fitted into various mathematical modeling equations to identify the release mechanism of the drug. The regression coefficients of F1–F7 for each of the algorithms are summarized in Table IV. The best-fit model for the formulations is based on the closeness of the regression coefficient to a value of 1. A model depicting a value closest to 1 among the formulations would demonstrate the appropriateness of that model in explaining the drug release mechanism. The zero-order and first-order models are based on systems where the drug release is independent and dependent on drug concentrations, respectively (42). The zero-order and first-order models used are shown in Eqs. 6 and 7 (43).

$$Q = K_0\ t \tag{6}$$

Where Q is the cumulative amount of drug released, K_0 is the zero-order constant, and t is the time.

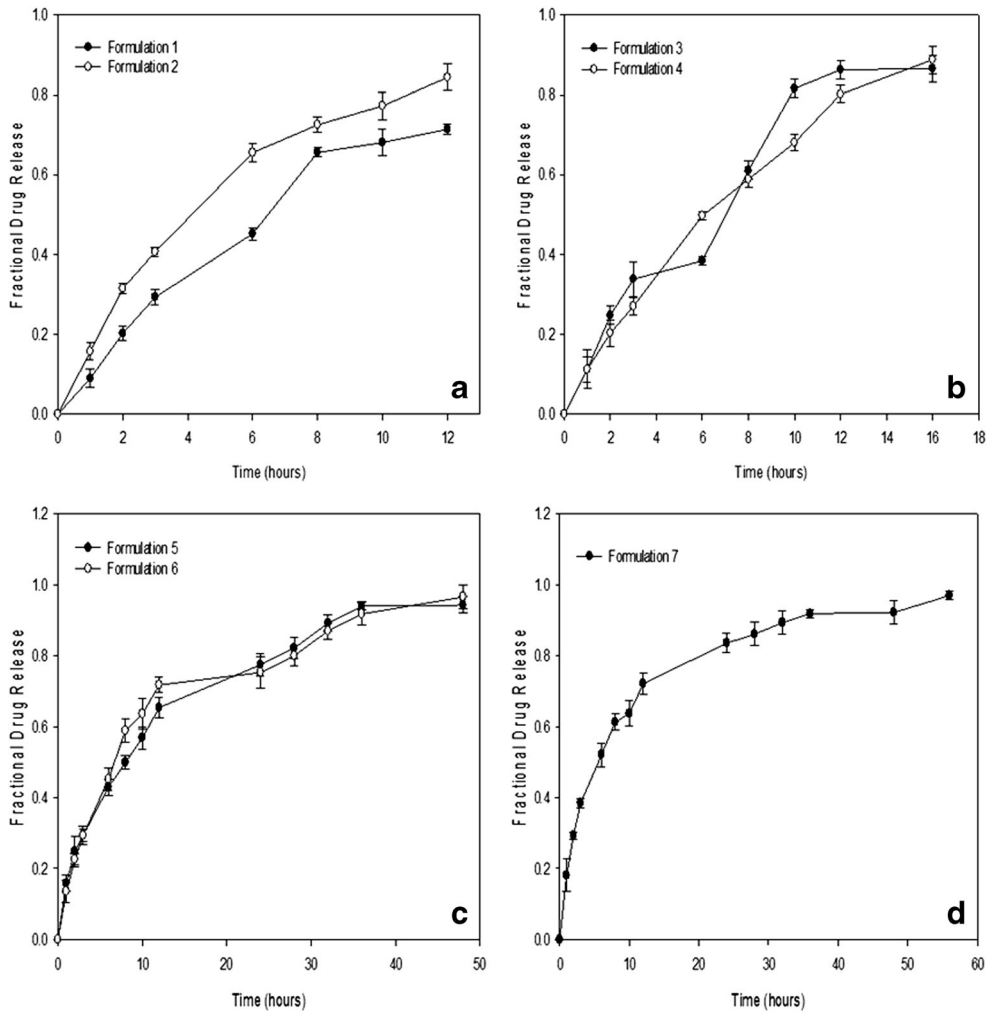

Fig. 10. Graphical representation of the fractional drug release of SMX from compressed matrix tablets F1–7. **a** F1–2 releases over a period of 12 h, **b** F3–4 releases over a period of 16 h, **c** F5–6 releases over a period of 48 h, and **d** F7 releases over a period of 56 h

Table IV. Mathematical Modeling of SMX Release from the Solid Dispersions

	Zero-order	First-order	Higuichi	
Formulation no.	Regression coefficient (R^2)	Regression coefficient (R^2)	Regression coefficient (R^2)	Best-fit model
F1	0.9473	0.8255	0.9795	Higuichi
F2	0.9295	0.8031	0.9824	Higuichi
F3	0.7107	0.6008	0.8497	Higuichi
F4	0.8063	0.6475	0.9372	Higuichi
F5	0.8693	0.7113	0.9669	Higuichi
F6	0.8042	0.6201	0.9226	Higuichi
F7	0.7641	0.5986	0.9079	Higuichi

The regression coefficients were elucidated for the zero-order model by plotting a graph of cumulative drug release (%) *versus* time based on *in vitro* drug release data.

$$\ln Q_t = \ln Q_0 K_0 t \tag{7}$$

Where Q_t is the cumulative amount of drug released, Q_0 is the initial amount of drug in the dissolution medium (usually zero), K_0 is the first-order constant, and t is the time. The regression coefficients for the first-order model was determined by plotting a graph of the log of cumulative release *versus* time based on data obtained from *in vitro* drug release.

Since the release of SMX was not concentration-dependent, it did not fit into the first-order release kinetic model as displayed in Table IV. Regardless of the nearness to linearity of the zero-order model, the results were not ideal and thus were not considered the best-fit model. In addition, the drug release data was fitted into the Higuichi model since it has been developed to describe the drug release from HPMC-based pharmaceutical delivery systems (44). The Higuichi model is the most commonly used method to describe the release rate of drug from a matrix system and is represented by Eq. 8 (45).

$$Q = K_H t^{1/2} \tag{8}$$

Where Q is the cumulative amount of drug released, K_H is the Higuichi dissolution constant, and t is the time. A plot of the cumulative percentage released *versus* the square root of time of the drug release data generated regression coefficients for the Higuichi model.

Based on the regression coefficients, the Higuichi model displayed the best linearity for majority of the formulations with an R^2 value of between 0.8497 and 0.9824, indicating that the drug release mechanism was based on a square root of a time-dependent process based on Fickian diffusion (46). Despite the Higuichi equation being the best-fit model, further mathematical analysis is required to obtain definite mechanistic deductions (44).

CONCLUSIONS

The menthol-based solid dispersions for improvement of the solubility and dissolution of SMX were successfully formulated as evidenced by the results obtained from physicochemical and physicomechanical characterization. SMX is used to treat various urinary tract pathogens and in combination with trimethoprim is considered the "gold standard" in the treatment of urinary tract infections (UTIs) (2). Thus, improvement in its solubility and dissolution is critical toward achieving optimal therapeutic effects. Characterization results confirmed successful formulation of the solid dispersions and its subsequent enhancement of the solubility and dissolution of SMX. A reduction in the particle size to the nanometer range for the solid dispersions resulted in an increased surface area and thus improved solubility and dissolution. Thermal analysis depicted a characteristic decrease in melting point for all the SMX-loaded solid dispersions. In addition, a decrease in the crystallinity and corresponding increase in the amorphous nature was apparent within the formulations as the concentration of menthol increased, thus allowing for the increase in the water affinity and solubility of SMX. Results from erosion, swelling, and solubility studies determined that the varying concentrations of menthol present within each formulation controlled the quantity of SMX released over time. The physicomechanical properties of MH and MR correlated with changes in crystallinity observed in the different formulations of SMX-loaded matrix tablets. Analysis of the molecular and vibrational transitions of the SMX-loaded solid dispersions determined the formation of new bonds resulting from the interaction between SMX and menthol. Solubility studies indicated the significant intrinsic increase in solubility of SMX as a component of the solid dispersions (998.75–1241.2 μg/mL) as compared to native SMX in SHIF pH 6.8 (790 μg/mL). In addition, *in vitro* drug release analysis displayed atypical, controlled drug release profiles for the various solid dispersions. This may be extremely useful within an oral drug delivery system where the properties of the system can be synchronously enhanced using a customizable solid dispersion. Selection of the best solid dispersion may be ascertained based on physicochemical, physicomechanical, drug release, and release-rate profiles desired to meet the needs of the particular drug delivery system. In addition, eutectic, monotectic, and peritectic transformation may be associated with a matrix solid dispersion system such as the menthol-SMX combination. However, achievement of these transformations would require further investigation and evaluation that would commence with basic phase studies to determine the composition at which the menthol-SMX combination would exist as a eutectic mixture.

ACKNOWLEDGMENTS

This study was funded by the National Research Foundation of South Africa.

Conflicts of Interest The authors confirm that there are conflicts of interest.

REFERENCES

1. Savjani KT, Gajjar AK, Savjani JK. Drug solubility: importance and enhancement techniques. ISRN Pharm. 2012. doi:10.5402/2012/195727.
2. Petri WA. Sulfonamides, trimethoprim-sulfamethoxazole, quinolones, and agents for urinary tract infections'. In: Chabner BA, Knollmann BC, editors. Goodman and Gilman's: the pharmacological basis of therapeutics. New York: McGraw-Hill; 2011. p. 252–88.
3. Dohrn R, Bertakis E, Behrend O, Voutsas E, Tassios D. Melting point depression by using supercritical CO_2 for a novel melt dispersion micronization process. J Mol Liq. 2007;131:53–9.
4. Sareen S, Mathew G, Lincy J. Improvement in solubility of poor water-soluble drugs by solid dispersion. Int J Pharm Investig. 2012;2:12–7.
5. Seedhar N, Agarwal P. Various solvent systems for solubility enhancement of enorfloxacin. Indian J Pharm Sci. 2009;71:82–7.
6. Liu D, Fei X, Wang S, Jiang T, Su D. Increasing solubility and dissolution rate of drugs via solid dispersions: itraconazole–poloxamer188 system. Asian J Pharm Sci. 2006;1:213–21.
7. Chiou WL, Riegelman S. Pharmaceutical applications of solid dispersion systems. J Pharm Sci. 1971;60:1281–302.
8. Luener C, Dressman J. Improving drug solubility for oral delivery using solid dispersions. Eur J Pharm Bio. 2000;50:47–60.
9. Vasconcelos T, Sarmento B, Costa P. Solid dispersions as strategy to improve oral bioavailability of poor water soluble drugs. Drug Discov Today. 2007;12:1068–75.
10. Sekiguchi K, Obi N. Studies on absorption of solid dispersions. I. A comparison of the behaviour of solid dispersions of sulphathiazole and that of ordinary sulphathiazole in man. Chem Pharm Bull. 1961;9:866–72.
11. Levy G. Effect of particle size on dissolution and gastrointestinal absorption rates of pharmaceuticals. Am J Pharm Sci. 1963;135:78–92.
12. Bhatnagar P, Dhote V, Mahajan SC, Mishra PK, Mishra DK. Solid dispersion in pharmaceutical drug development: from basics to clinical applications. Curr Drug Deliv. 2014;11:155–71.
13. Lindenburg M, Kopp S, Dressman JB. Classification of orally administered drugs on the World Health Organization model list of essential medicines according to the biopharmaceutics classification system. Eur J Pharm Biopharm. 2004;58:265–78.
14. Saffoon N, Uddin R, Huda NH, Sutradhar KB. Enhancement of oral bioavailability and solid dispersion: a review. J Appl Pharm Sci. 2011;1:13–20.
15. Reynolds JEF. Martindale: the extra pharmacopoeia. London: Pharmaceutical Press; 1993. p. 154–209.
16. Williams RO, Watts AB, Miller DA. Formulating poorly water soluble drugs. New York: Springer; 2012. p. 526–9.
17. Lee MY, Kim MY, Kim S, Lee J. Cryoprotectants for freeze drying of drug nano-suspensions: effect of freezing rate. J Pharm Sci. 2009;98:4808–17.
18. Thakur R, Gupta RB. Rapid expansion of supercritical solution with solid cosolvent (RESS-SC) process: formation of 2-aminobenzoic acid nanoparticle. J Supercrit Fluids. 2006;37:307–15.
19. Efentakis M, Vlachou M. Evaluation of high molecular weight poly(oxyethylene) (Polyox)polymer: studies of flow properties and release rates of furosemide and captopril from controlled-release hard gelatin capsules. Pharm Develop Technol. 2000;5:339–46.
20. Sathish U, Syed IA. Formulation and characterization of matrix and triple layer matrix tablets for controlled delivery of tramadol hydrochloride. Int J Pharm Sci. 2013;5:458–64.
21. McGlinchey D. Characterisation of bulk solids. Oxford: Blackwell Publishing Ltd; 2005. p. 50–2.
22. Gabbott P. Principles and applications of thermal analysis. Oxford: Blackwell Publishing Ltd; p. 17–40.
23. Widmann J, Schubnell M, Riesen R, Schawe J, Darribére C, Jörimann U. Interpreting DSC curves: part 2: isothermal measurements. UserCom. 2000;2:1–10.
24. Neubert R, Rettig W, Wartewig S, Wegener M, Wienhold A. Structure of stratum corneum lipids characterized by FT-Raman spectroscopy and DSC. II. mixtures of ceramides and saturated fatty acids. Chem Phys Lipids. 1997;89:3–14.
25. Yamashita K, Nakate T, Okimoto K, Ohike A, Tokunagu Y, Ibuki R, *et al.* Establishment of new preparation method for solid dispersion formulation of tacrolimus. Int J Pharm. 2003;267:79–91.
26. Sinha S, Ali M, Baboota S, Ahuja A, Kumar A, Ali J. Solid dispersion as an approach for bioavailability enhancement of poorly water-soluble drug ritonavir. AAPS PharmSciTech. 2010;11:518–27.
27. Sharma A, Jain CP, Tanwar YS. Preparation and characterization of solid dispersions of carvedilol with poloxamer 188. J Chil Chem Soc. 2013;58:1553–7.
28. Tantishaiyakul V, Kaewnopparat N, Ingkatawornwong S. Properties of solid dispersions of piroxicam in polyvinylpyrrolidone. Int J Pharm. 1999;181:143–51.
29. Widmann J, Schubnell M, Riesen R, Schawe J, Darribére C, Jörimann U. Interpreting TGA curves. UserCom. 2001;1:1–20.
30. Coates J. Interpretation of infrared spectra, a practical approach. Chichester: Wiley; 2000. p. 10815–37.
31. Stoker HS. Organic and biological chemistry. Belmont: Brooks/Cole Cengage Learning; 2013. p. 83–128.
32. Pillay V, Fassihi R. In vitro release modulation from crosslinked pellets for site-specific drug delivery to the gastrointestinal tract: II. Physicochemical characterization of calcium–alginate, calcium–pectinate and calcium–alginate–pectinate pellets. J Control Release. 1999;59:243–56.
33. Johnson AW. Invitation to organic chemistry. Canada: Jones and Bartlett Publishing; 1999. p. 543–6.
34. Council of Europe. The European pharmacopoeia. France: Maisonneuve S.A; 2001. p. 723–7.
35. Sethia S, Squillante E. Solid dispersion of carbamazepine in PVP K30 by conventional solvent evaporation and supercritical methods. Int J Pharm. 2004;272:1–10.
36. Won D, Kim M, Lee S, Park J, Hwang S. Improved physicochemical characteristics of felodipine solid dispersion particles by supercritical anti-solvent precipitation process. Int J Pharm. 2005;301:199–208.
37. Hattori Y, Haruna Y, Otsuka M. Dissolution process analysis using model-free Noyes-Whitney integral equation. 2013; 102: 227–31.
38. Martin A. Physical pharmacy: physical chemical principles in the pharmaceutical sciences. Philadelphia: Lea and Febiger; 1993. p. 41–2.
39. Ratner BR, Hoffman AS, Schoen FJ, Lemons JE. Biomaterials science: an introduction to materials in medicine. Oxford: Elsevier; 2012. p. 187–94.
40. Roni MA, Kibria G, Jalil R. Formulation and in vitro evaluation of alfusozin extended release tablets using directly compressible eudragit. Indian J Pharm Sci. 2009;71:252–8.
41. Wadher KJ, Kakde RB, Umekhar MJ. Study on sustained-release metformin hydrochloride from matrix tablet: influence of hydrophilic polymers and in vitro evaluation. Int J Pharm Investig. 2011;1:157–63.
42. Singh V, Singh M. Review: in-vitro drug release characterization models. Int J Pharm Stud Res. 2011;2:77–84.
43. Siepmann J, Siepmann F. Mathematical modeling of drug delivery. Int J Pharm. 2008;364:328–43.
44. Siepmann J, Peppas NA. Modeling of drug release from delivery systems based on hydroxypropyl methylcellulose (HPMC). Adv Drug Deliv Rev. 2012;64:163–74.
45. Merchant H, Shoaib H, Tazeen J, Yousuf R. Once-daily tablet formulation and in vitro release evaluation of cefpodoxime using hydroxypropyl methylcellulose: a technical note. AAPS PharmSciTech. 2006;7:178–83.
46. Yadav G, Bansal M, Thakur N, Khare S, Khare P. Multilayer tablets and their drug release kinetic models for oral controlled drug delivery system. ME J Sci Res. 2013;16:782–95.
47. Arnikar AJ, Kadam SS, Gujar KN. Essentials of physical chemistry and pharmacy. Orient Longman Limited: Bombay; 1992.